Environmental Processes (2026) 13:7
https://doi.org/10.1007/s40710-026-00819-0

RESEARCH

Heavy Metals Bioaccumulation in Riparian Vegetation: A Multi-Species Biomonitoring Framework Using Total X-Ray Reflection Fluorescence Spectroscopy

Shakeel Ahmed Talpur[1,2,3] · Simonetta Cristina Di Simone[4] · Aziz Ahmed[5] · Hafeez Ahmed Talpur[6] · Muhammad Yousuf Jat Baloch[7] · Francesco Stoppa[1,2] · Luigi Menghini[4] · Beatrice Maria Sole Giambastiani[3] · Gianluigi Rosatelli[1,2]

Received: 28 October 2025 / Accepted: 23 January 2026

Abstract

Heavy metal contamination in Mediterranean riparian ecosystems presents serious risks to biodiversity and human health, requiring innovative biomonitoring methods for polluted watersheds. This study developed a comprehensive biomonitoring framework for an industrially impacted Mediterranean river basin, with approximately 100,000 tons of contaminated waste in landfills from decades of metallurgical processing. We investigated heavy metal bioaccumulation patterns in five taxonomically diverse native riparian species (*Equisetum arvense*, *Laurus nobilis*, *Rubus ulmifolius*, *Sambucus nigra*, and *Salix alba*) across contaminated and reference sites using Total Reflection X-ray Fluorescence (TXRF) spectroscopy. TXRF was validated against Inductively Coupled Plasma Atomic Optical Spectroscopy (ICP-AOS) using standard reference materials, demonstrating superior sensitivity for trace element detection in plant matrices. Heavy metal concentrations varied significantly among species and sites in riparian vegetation, with Fe (23.14 ± 5.21 mg/kg), Mn (2.74 ± 0.89 mg/kg), and Cr (3.33 ± 1.12 mg/kg) showing the highest accumulation. *Laurus nobilis* appeared as a multi-metal hyperaccumulator with the highest Pollution Load Index (PLI = 2.67) and exceptional accumulation of Cr (14.74 mg/kg) and Fe (63.64 mg/kg). Statistical analysis (Kruskal-Wallis test, $p < 0.05$) confirmed that Mn and Cr represented primary anthropogenic pollutants, with contaminated sites showing 2.20-fold and 1.92-fold increases, respectively. Principal Component Analysis revealed distinct co-accumulation networks, with Fe-Cr-Ni-Cu forming synchronized uptake mechanisms, while Mn operated independently. Biogeochemical ratio analyses (Fe/Zn, Cu/Mn) provided sensitive contamination indicators, detecting physiological stress beyond simple concentration measurements. Results support species-specific phytoremediation strategies aligned with UN Sustainable Development Goals, with *Laurus* suitable for multi-metal extraction and *Equisetum* for Mn-specific remediation, advancing sustainable environmental management in industrially impacted Mediterranean watersheds.

Highlights

- TXRF spectroscopy outperforms ICP-AOS for trace metals in plant tissues.

Extended author information available on the last page of the article

Published online: 07 February 2026

- Laurus nobilis exhibits multi-metal hyperaccumulation capacity (PLI = 2.67).
- Mn and Cr show 2.20-fold and 1.92-fold increases at contaminated sites.
- Fe-Cr-Ni-Cu co-accumulate while Mn operates independently.
- Biogeochemical ratios detect physiological stress in riparian plants.

Keywords Riparian vegetation biomonitoring · Multi-element accumulation patterns · Pescara river basin · Mediterranean ecosystem contamination · Total reflection x-ray fluorescence (TXRF)

1 Introduction

Heavy metal contamination represents a pervasive and persistent environmental hazard of global concern, impacting terrestrial and aquatic ecosystems across industrialized and developing regions, with demonstrable risks to biodiversity, ecological functioning, and human health (Jat Baloch et al. 2023; Talpur et al. 2025b; Ogwu et al. 2025a; Liu et al. 2025a). Unlike most organic pollutants, heavy metals are non-biodegradable and undergo long-term environmental persistence, progressively accumulating within soils, sediments, and biological tissues, and biomagnifying through trophic networks (Ogwu et al. 2025a; Asare et al. 2025; Khan et al. 2025a). Current estimates indicate that anthropogenic emissions, including heavy metals from industrial processes, mining activities, and combustion of fossil fuels, exceed natural geochemical fluxes by factors of 5–20, primarily because of intensive mining, metallurgical processing, industrial effluents, and fossil fuel combustion (Baloch et al. 2020, 2025; Natasha et al. 2020; Talpur et al. 2020, 2024). The Mediterranean basin, supporting more than 500 million inhabitants and classified as a global biodiversity hotspot, is particularly susceptible due to its concentration of industrial activities and semi-arid climatic regime, which promotes the retention of contaminants during extended drought periods and their episodic remobilization during precipitation events (Palma et al. 2021; Intergovernmental Panel On Climate Change (Ipcc) 2023; Neumann et al. 2025; Haydous et al. 2025). Riparian ecosystems, functioning as ecotonal interfaces between terrestrial and lotic systems, are integral to hydrological regulation, biodiversity maintenance, and the provision of critical ecosystem services, including nutrient retention, water filtration, and habitat connectivity (Dodds et al. 2025; Dinca et al. 2025). Globally, these systems operate as sentinel zones for detecting watershed contamination, receiving inputs via overland flow, subsurface hydrological pathways, atmospheric deposition, and fluvial inundation (Leibowitz et al. 2023). Riparian vegetation exhibits morphological and physiological adaptations conducive to the uptake, translocation, and sequestration of heavy metals from contaminated matrices. Consequently, riparian corridors are designated priority monitoring units within international environmental policy frameworks, including the European Water Framework Directive and the United Nations Sustainable Development Goals (Alvarez et al. 2021).

Biomonitoring through plant tissues supplements conventional monitoring techniques by capturing pollutant exposure over prolonged durations and delivering spatially refined contamination assessments (Bellino et al. 2020; Tarish et al. 2024; Khan et al. 2025a). Vegetation functions as a biological filter, sequestering contaminants to their bioavailable concentrations, thereby acting as living records of both present and past pollution events

(Bessonova and Sklyarenko 2020). Numerous plant species are reliable indicators of heavy metal contamination, often exhibiting strong correlations between environmental concentrations and tissue levels of cadmium, chromium, copper, lead, nickel, and zinc (Xing et al. 2020; Cakaj et al. 2024). While several studies have examined metal accumulation in Mediterranean riparian species, including work by (Tőzsér et al. 2023) on Populus and Salix species and (Papazoglou et al. 2025) on contaminated floodplains, comprehensive multi-species assessments comparing accumulation strategies across diverse taxonomic groups remain limited (Popa et al. 2019). Existing research has primarily concentrated on individual species or temperate-zone ecosystems, leaving gaps in understanding the relative performance of different taxonomic groups in Mediterranean environments (Cakaj et al. 2024). Furthermore, the interactions of multiple metals within plant tissues are rarely addressed, despite evidence that synergistic and antagonistic relationships can modulate uptake and toxicity (Gong et al. 2020; Jat Baloch et al. 2021; Zhao et al. 2024). Analytical investigations typically employ Inductively Coupled Plasma Optical Emission Spectroscopy (ICP-OES) and Inductively Coupled Plasma Mass Spectrometry (ICP-MS) for high-sensitivity quantification, along with Atomic Absorption Spectroscopy (AAS), Flame Atomic Absorption Spectroscopy (FAAS), and Graphite Furnace Atomic Absorption Spectroscopy (GFAAS) for targeted elemental detection. X-ray based techniques, such as Total Reflection X-ray Fluorescence (TXRF), enable minimal sample preparation and simultaneous multi-element detection. However, systematic comparative assessments of these methods for plant tissue analysis remain limited (Rawat et al. 2024; Talpur et al. 2025a).

The Pescara River basin in central southern Italy highlights the severe environmental pressures on Mediterranean river systems, where decades of metallurgical processing, chemical manufacturing, and improper waste disposal have caused ongoing contamination that threatens ecosystem health and water security (Talpur et al. 2025a). Industrial activities, particularly in Bussi sul Tirino, have left three large landfills designated as Sites of National Interest containing ~ 100,000 tons of industrial waste, with heavy metals entering riparian ecosystems via landfill leachates, groundwater flow, and surface transport. Current monitoring, relying on conventional water and sediment sampling, is limited in capturing the spatial and temporal information of contamination, as water sampling offers only instantaneous and seasonally variable snapshots, and sediment analysis may overlook bioavailable metal fractions critical to ecosystem health (Vitali et al. 2021; Castellani et al. 2021). The complex hydro-geomorphological dynamics of this basin require innovative methods integrating spatial and temporal contamination data, while the lack of baseline information on native riparian species' metal accumulation hampers management, and its critical role in agricultural and domestic water supply heightens the urgency for accurate pollution characterization to protect ecosystem and human health (Iqbal et al. 2021; Talpur et al. 2024, 2025a, b; Shtull-Trauring et al. 2025).

This study aimed to establish a comprehensive biomonitoring framework for assessing heavy metal contamination in Mediterranean riparian ecosystems by integrating native plant community analyses with advanced analytical techniques. Specifically, it seeks to quantify and compare heavy metal concentrations in leaf tissues of five taxonomically diverse native riparian species across contaminated and reference sites within the Pescara River basin to establish baseline accumulation data and characterize species specific patterns. The study also evaluates the performance of Total Reflection X-ray Fluorescence spectroscopy relative to conventional techniques for trace element determination in plant matrices and

assesses contamination gradients using established environmental indices to quantify pollution severity and distinguish anthropogenic from natural sources. Additionally, it identifies metal co-accumulation patterns and species-specific sequestration strategies to elucidate relationships between different metals and group species by their accumulation profiles. Finally, it evaluates biogeochemical indicators of ecosystem health while exploring potential phytoremediation applications aligned with United Nations Sustainable Development Goals, demonstrating the practical relevance of biomonitoring research for addressing global environmental challenges.

Moreover it makes three key contributions to the field: (1) the first systematic comparison of TXRF versus ICP-AOS performance for multi-element analysis in diverse riparian plant matrices, establishing TXRF as a better technique for biomonitoring applications; (2) novel baseline data on metal accumulation capacities of five taxonomically diverse Mediterranean riparian species, enabling species specific phytoremediation recommendations; and (3) the development of biogeochemical ratio indicators (Fe/Zn, Cu/Mn) as sensitive early-warning tools for detecting ecosystem stress beyond conventional concentration thresholds. These findings have broad applicability to contaminated watersheds worldwide and advance the scientific basis for nature based remediation strategies aligned with circular economy principles.

2 Methodology

2.1 Study Area and Site Selection

The Pescara River basin in the Abruzzo region of southern Italy includes the interconnected Aterno and Tirino Rivers, flowing northeast to southwest through urban and industrial areas. A major pollution hotspot is the Bussi sul Tirino industrial estate, which contains metallurgical, chemical, and electroplating facilities along with three large landfills (Talpur et al. 2025a). The most contaminated, “2A and 2B” and “Tre Monti” Sites of National Interest (SIN), hold about 100,000 t of industrial waste from past activities and improper disposal. Leachate and groundwater spread heavy metals into surrounding ecosystems. The basin’s limestone and detrital geology promote contaminant mobility and downstream transport (Vitali et al. 2021). Sampling sites were S1 at 42.194273° N, 13.851151° E, located 500 m downstream of significant industrial discharges near “Tre Monti,” and S2 at 42.174247° N, 13.830101° E, a reference site 4.5 km upstream near the Pescara River springs with minimal industrial influence but similar geology, as shown in (Fig. 1).

2.2 Plant Species Selection and Sample Collection

Five riparian plant species were chosen based on (1) consistent presence at both study sites, (2) documented ability to accumulate heavy metals, and (3) representation of distinct taxonomic groups: *Equisetum arvense* L. (horsetail), *Laurus nobilis* L. (bay laurel), *Rubus ulmifolius* Schott (blackberry), *Sambucus nigra* L. (elderberry), and *Salix alba* L. (white willow). The selection was persistent on native Mediterranean taxa that show bioaccumulation capacity and are widely distributed across contaminated and reference sites. Leaf material was collected in July 2024 to reduce seasonal variation. At each site, mature, fully expanded

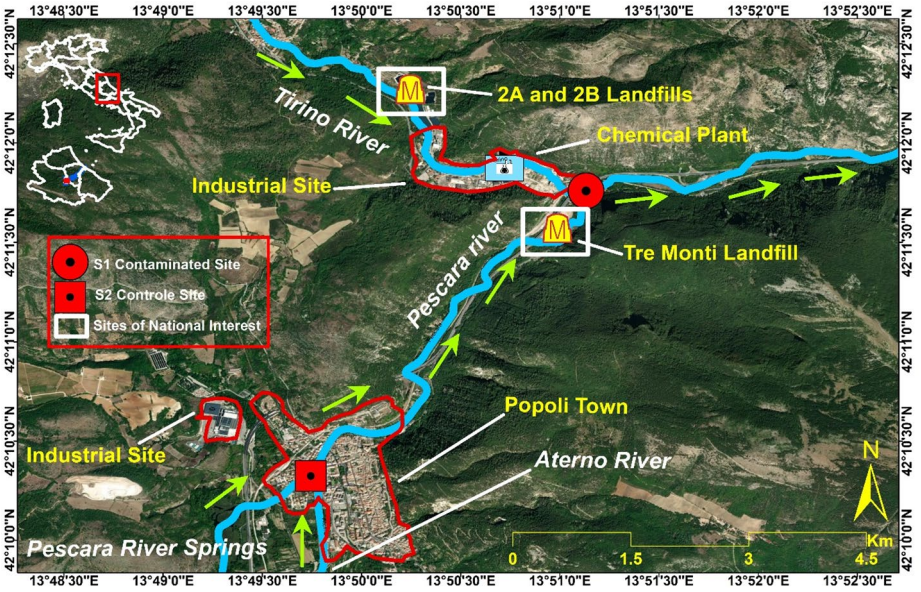

Fig. 1 Study area map showing sampling sites (S1: contaminated site, marked with red circle; S2: reference site, marked with red square), industrial facilities, landfill locations (white bounding box indicates Sites of National Interest), and river flow direction. Base map: ESRI World Imagery; coordinate system: WGS 84

leaves were sampled from $n = 3–5$ individual plants per species within a 50 m radius of the central GPS coordinate. Only healthy, undamaged leaves from the growing season were collected using sterilized stainless-steel scissors. Individual leaves were pooled into a composite sample (20–30) for each species-site combination to ensure enough biomass and capture site-level variability. Samples were placed in pre-cleaned polyethylene bags labeled with unique identifiers and transported to the laboratory within 4 h of collection.

2.3 Sample Preparation and Analysis

Leaf samples were rinsed three times with distilled water to remove surface particulates, then dried in a ventilated chamber at 40 °C with forced air circulation in the dark for 72–96 h, until a constant weight was achieved. From each dried sample, 0.500 ± 0.001 g (dry weight) was accurately weighed and homogenized with 20 mL of Milli-Q ultrapure water using an IKA T25 digital ULTRA-TURRAX homogenizer (IKA-Werke GmbH, Staufen, Germany) operating at 10,000 rpm for 2 min to produce a uniform plant suspension. An aliquot of 1.0 mL from each homogenate was combined with 7.0 mL of Milli-Q water and 2.0 mL of concentrated nitric acid (67% HNO_3, Suprapur grade, Merck) for organic matter digestion, facilitating the release of heavy metals into solution. Samples were analyzed without filtration to maintain the integrity of the sample matrix. Heavy metal concentrations were determined using Total Reflection X-ray Fluorescence (TXRF) spectrometry (Horizon TXRF spectrometer, G.N.R. Analytical Instruments, Novara, Italy) equipped with a 900 W Mo-Kα X-ray source (17.44 keV) and a Silicon Drift Detector (SDD, 30 mm^2 active area, energy resolution < 145 eV at 5.9 keV). Gallium, at 10 mg L^{-1} (1000 µg L^{-1} Ga standard solution,

Sigma-Aldrich), was added as an internal standard to correct for matrix effects and enhance accuracy. Target elements (Cr, Cu, Fe, Mn, Ni, Ti, Zn) were quantified at 900 s per sample. Measurements were performed in triplicate for each sample, and results are reported as mean ± standard deviation. The analytical procedure followed the ISO 17,025 guidelines for trace element analysis in biological matrices.

2.4 Quality Control and Method Validation

Method performance was evaluated through parallel analysis, using Inductively Coupled Plasma–Atomic Optical Spectroscopy (ICP-AOS, Thermo Scientific iCAP 7400 Duo, Thermo Fisher Scientific, Waltham, MA, USA) as the reference technique, with identical sample preparation protocols applied to both methods. Method accuracy was verified using NIST Standard Reference Material 1515 (Apple Leaves) and NIST SRM 1570a (Spinach Leaves), with recoveries ranging from 92% to 108% for all target elements, confirming the reliability of both analytical methods. Comparative results demonstrated substantial differences in analytical performance. Total Reflection X-ray Fluorescence (TXRF) quantified 70 measurements (five species × seven elements × two sites) without producing negative values. Meanwhile, ICP-AOS yielded negative concentrations in 34 out of 70 measurements (48.6%), which occurred because the sample preparation protocol, while optimized for TXRF analysis, resulted in matrix conditions that interfered with ICP-AOS detection for certain elements at trace concentrations. This limitation was most apparent for Cr, Cu, and Ni, where 8 of 10 samples showed negative values, and for Ti, where all measurements were below the detection limit, as shown in (Table 1). According to the results, TXRF provided measurable concentrations for each target element. Detection limits for TXRF ranged from 0.03 to 0.26 mg/kg depending on the element (see Table 1), while ICP-AOS detection limits ranged from 0.00 to 2.92 mg/kg. These findings demonstrate that TXRF has higher analytical sensitivity and better matrix tolerance than ICP-AOS for detecting trace elements in plant tissue, supporting its selection as the preferred method for this biomonitoring study.

2.5 Toxic Signatures, Statistical Measures, and Visualizations

Heavy metal contamination in plant tissues was assessed using pollution and risk indicators. The Contamination Factor (CF) is a unitless measure that indicates contamination severity by comparing the concentration of each metal at the study site (C_i, mg/kg) to its background level from a reference site ($C_{background}$, mg/kg), as shown in Eq. 1 (Talpur et al. 2025a). Background concentrations were derived from measurements at the reference site (S2), which represents uncontaminated conditions with similar geological characteristics to the contaminated site, following established biomonitoring protocols (Maeyouf et al. 2025; Heta et al. 2025). Classification criteria for CF are listed in (Table 2).

$$CF = \frac{C_i}{C_{background}} \tag{1}$$

The Pollution Load Index (PLI) combines contamination data from multiple metals by calculating the geometric mean of their individual CF values (CF_i) across (n) analyzed metals.

Table 1 Comparison of TXRF and ICP-AOS methods for trace element analysis in plant species. Values represent concentration; quantities in parentheses indicate limits of detection (LOD) for each method and element; < LOD = below detection limit

Species	Site	Method	Cr (mg/kg)	Cu (mg/kg)	Fe (mg/kg)	Mn (mg/kg)	Ni (mg/kg)	Ti (mg/kg)	Zn (mg/kg)
Equisetum	S1	TXRF	2.14 (0.13)	0.66 (0.05)	20.50 (0.08)	10.21 (0.09)	1.33 (0.06)	3.67 (0.21)	6.40 (0.05)
		ICP-AOS	< LOD (0.01)	< LOD (0.03)	12.97 (0.19)	12.99 (0.21)	< LOD (0.14)	< LOD (2.92)	2.92 (0.01)
Equisetum	S2	TXRF	2.26 (0.14)	0.85 (0.06)	22.21 (0.10)	2.97 (0.11)	2.14 (0.07)	2.57 (0.26)	11.45 (0.06)
		ICP-AOS	< LOD (0.09)	< LOD (0.02)	9.97 (0.22)	1.59 (0.03)	< LOD (0.04)	< LOD (1.54)	3.18 (0.02)
Laurus	S1	TXRF	14.74 (0.14)	1.20 (0.05)	63.64 (0.09)	3.28 (0.10)	5.64 (0.05)	5.86 (0.22)	8.77 (0.06)
		ICP-AOS	< LOD (0.03)	< LOD (0.03)	10.04 (0.08)	1.37 (0.02)	< LOD (0.13)	< LOD (1.09)	3.07 (0.04)
Laurus	S2	TXRF	4.11 (0.08)	0.76 (0.03)	21.45 (0.05)	0.68 (0.05)	2.22 (0.04)	2.24 (0.13)	4.54 (0.04)
		ICP-AOS	< LOD (0.06)	< LOD (0.02)	9.12 (0.21)	0.48 (0.01)	< LOD (0.07)	< LOD (0.70)	2.45 (0.04)
Rubus	S1	TXRF	2.90 (0.10)	0.78 (0.04)	23.39 (0.07)	1.45 (0.07)	1.81 (0.05)	1.81 (0.17)	4.63 (0.04)
		ICP-AOS	< LOD (0.04)	0.10 (0.02)	21.94 (0.66)	2.00 (0.04)	0.12 (0.21)	< LOD (0.20)	3.15 (0.17)
Rubus	S2	TXRF	2.62 (0.07)	0.63 (0.03)	23.04 (0.03)	1.11 (0.05)	2.43 (0.03)	0.73 (0.12)	4.91 (0.03)
		ICP-AOS	< LOD (0.02)	0.03 (0.02)	30.69 (0.60)	1.50 (0.03)	1.04 (0.22)	< LOD (0.79)	2.11 (0.02)
Sambucus	S1	TXRF	1.39 (0.11)	0.40 (0.04)	15.78 (0.07)	2.82 (0.08)	1.47 (0.05)	2.39 (0.19)	5.21 (0.05)
		ICP-AOS	4.81 (0.17)	< LOD (0.03)	25.94 (0.53)	3.90 (0.06)	< LOD (0.48)	< LOD (1.24)	1.82 (0.04)
Sambucus	S2	TXRF	1.43 (0.12)	0.60 (0.05)	19.41 (0.07)	1.99 (0.08)	1.30 (0.05)	1.86 (0.20)	5.23 (0.05)
		ICP-AOS	0.05 (0.04)	< LOD (0.06)	27.52 (0.66)	2.78 (0.03)	< LOD (0.05)	< LOD (0.75)	2.69 (0.13)
Salix	S1	TXRF	0.68 (0.12)	0.48 (0.04)	9.66 (0.08)	1.10 (0.09)	0.53 (0.05)	1.48 (0.19)	4.28 (0.05)
		ICP-AOS	< LOD (0.01)	< LOD (0.03)	6.25 (0.11)	1.27 (0.00)	< LOD (0.07)	< LOD (0.77)	2.92 (0.08)
Salix	S2	TXRF	0.99 (0.10)	0.61 (0.04)	12.32 (0.06)	1.82 (0.07)	0.57 (0.04)	1.84 (0.17)	6.16 (0.04)
		ICP-AOS	< LOD (0.05)	< LOD (0.03)	9.68 (0.34)	2.00 (0.06)	< LOD (0.03)	< LOD (1.15)	3.96 (0.05)

Table 2 Classification ranges and interpretation criteria for contamination factor (CF), pollution load index (PLI), enrichment factor (EF), and ecological risk index (ERI)

Index	Value Range	Interpretation
CF	CF < 1	Low contamination
	1 ≤ CF < 3	Moderate contamination
	3 ≤ CF < 6	Considerable contamination
	CF ≥ 6	Very high contamination
PLI	PLI ≤ 1	No pollution
	PLI > 1	Pollution
EF	EF < 2	Minimal enrichment
	2 ≤ EF < 5	Moderate enrichment
	5 ≤ EF < 20	Significant enrichment
	20 ≤ EF < 40	Very high enrichment
	EF ≥ 40	Extremely high enrichment
ERI	ERI < 150	Low ecological risk
	150 ≤ ERI < 300	Moderate ecological risk
	300 ≤ ERI < 600	Considerable ecological risk
	ERI ≥ 600	Very high ecological risk

This overall index reflects the pollution level of a site, calculated by Eq. 2 (Talpur et al. 2025a), with interpretive guidelines provided in (Table 2).

$$PLI = (CF_1 \times CF_2 \times CF_3 \times \ldots \times CF_n)^{\wedge}(1/n) \tag{2}$$

Enrichment Factor (EF) distinguishes between natural and human-made sources by comparing the metal-to-iron ratio in the sample to that in background material. The parameter uses the concentrations of the heavy metal of interest ($C_{\text{Heavy metal}}$, mg/kg) and iron (C_{Fe}, mg/kg) as a conservative tracer to account for natural geochemical variability, as demonstrated in Eq. 3 (Kawałko et al. 2023). EF interpretative ranges are listed in (Table 2).

$$EF = \frac{\left(\frac{C_i}{C_{ref}}\right) sample}{\left(\frac{C_i}{C_{ref}}\right) background} \tag{3}$$

Ecological Risk Index (ERI) estimates the potential environmental hazard of heavy metal contamination by integrating metal enrichment levels with their respective toxic-response factors (T_i). This index incorporates the product of the toxicity coefficient (T_i) and enrichment factor (EF_i) for each heavy metal, with summation across all analyzed metals as presented in Eq. 4 (Talpur et al. 2025a). Classification criteria are provided in (Table 2).

$$ERI = \sum_{i=1}^{n} (T_i \times EF_i) \tag{4}$$

Statistical analyses were performed using R (4.3.0) and ArcGIS Pro (10.8) for geospatial visualization. Descriptive statistics summarized metal concentrations, while Principal Component Analysis (PCA) identified co-accumulation patterns. Spearman correlation analysis assessed relationships among metals, and contamination indices (CF, PLI, EF, ERI) quantified site-specific risks. Non-parametric Kruskal-Wallis tests were used to assess significant differences in metal concentrations between sites and among species, with Dunn's post-

hoc test for pairwise comparisons (significance level $\alpha = 0.05$). Effect sizes were calculated using eta-squared (η^2). Visualization outputs included bar plots, heatmaps, radar plots, PCA biplots, and correlation matrices to facilitate interpretation and biomonitoring assessment.

3 Results and Discussion

3.1 Heavy Metal Accumulation Patterns

Heavy metal concentrations in riparian plant leaf tissues demonstrated significant variation among species and between contaminated (S1) and reference (S2) sites (Fig. 2). Kruskal-Wallis tests established significant differences between sites for Mn ($H = 4.82$, $p = 0.028$, $\eta^2 = 0.42$) and Cr ($H = 3.91$, $p = 0.048$, $\eta^2 = 0.34$), while differences for other elements approached significance ($p < 0.10$). Fe exhibited the highest mean concentration at 23.14 ± 14.21 mg/kg (range: 9.66–63.64 mg/kg, CV = 61.4%), followed by Mn at 2.74 ± 2.63 mg/kg (0.68–10.21 mg/kg, CV = 95.7%) and Cr at 3.33 ± 3.92 mg/kg (0.68–14.74 mg/kg, CV = 117.9%). Zn averaged 6.16 ± 2.16 mg/kg (4.28–11.45 mg/kg, CV = 35.1%), while Cu, Ni, and Ti were lower at 0.70 ± 0.22, 1.94 ± 1.48, and 2.44 ± 1.44 mg/kg, respectively. Site specific analyses revealed consistently higher concentrations at the contaminated site (S1) compared to the reference site (S2), with Fe at 26.59 mg/kg versus 19.69 mg/kg (1.35-fold increase), Cr at 4.37 mg/kg versus 2.28 mg/kg (1.92-fold increase, $p = 0.048$), and Ni at 2.15 mg/kg versus 1.73 mg/kg (1.24-fold increase). Mn showed the most significant difference, with 3.77 mg/kg at S1 compared to 1.71 mg/kg at S2 (2.20-fold increase, $p = 0.028$), demonstrating substantial industrial influence on metal contamination levels (Qadir et al. 2021; Koç et al. 2024).

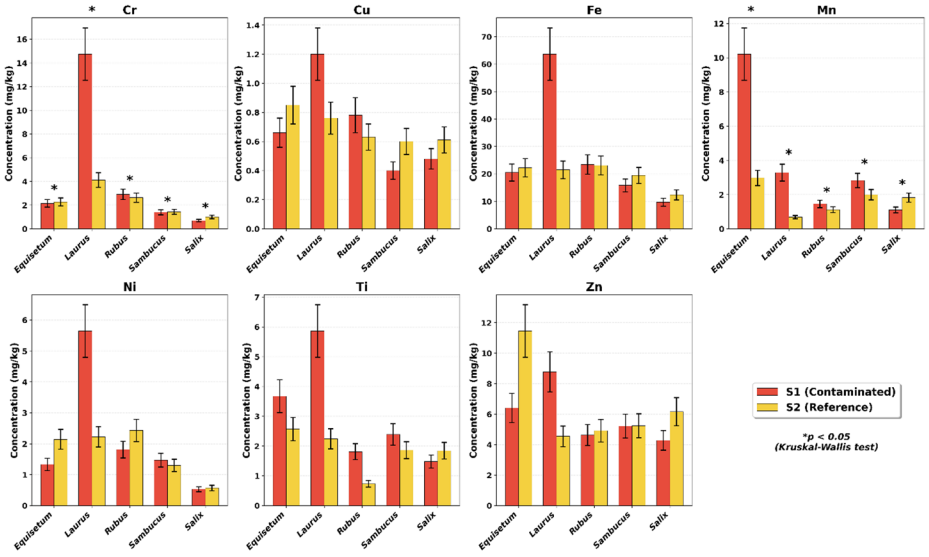

Fig. 2 Heavy metal concentrations (mg/kg) in leaf tissues of riparian plant species from contaminated (S1, red) and reference (S2, yellow) sites. Species: *Equisetum*, *Laurus*, *Rubus*, *Salix*, and *Sambucus*. Error bars represent standard deviation of triplicate measurements. Asterisks indicate statistically significant differences between sites (*$p < 0.05$, Kruskal-Wallis test)

Species-specific accumulation patterns revealed distinct physiological strategies for heavy metal handling (Lin et al. 2025; Andersone-Ozola et al. 2025; Asare et al. 2025). *Laurus* recorded the highest levels for several heavy metals, particularly Cr (14.74 mg/kg), Fe (63.64 mg/kg), and Ni (5.64 mg/kg) at the contaminated site, suggesting its potential as a hyperaccumulator. *Equisetum* exhibited the highest Mn concentration at S1 (10.21 mg/kg) but moderate levels for other heavy metals, while *Salix* generally had the lowest concentrations across most elements, indicating lower uptake capacity or stronger exclusion mechanisms. Hierarchical clustering analysis (Fig. 3) revealed clear patterns in heavy metal concentration profiles. *Laurus* from the contaminated site formed a distinct and isolated cluster due to its exceptionally high concentrations of several heavy metals. The analysis presented a strong site-specific contamination gradient, particularly for Mn and Zn, where S1 samples consistently grouped separately from S2 samples. Variability analysis supported these trends, with Mn having the highest coefficient of variation (CV = 95.7%) due to pronounced site differences and species-specific accumulation patterns, while Cr also exhibited substantial variability (CV = 117.9%), mainly driven by unusually high concentrations in *Laurus* at the contaminated site.

Analysis of metal sequestration strategies revealed distinct species-specific approaches to heavy metal accumulation in leaf tissues (Figs. 4 and 5). Total metal burden calculations demonstrated that *Laurus* exhibited the highest overall sequestration capacity with a mean total burden of 69.56 mg/kg across both sites, followed by *Equisetum* (44.67 mg/kg), *Rubus* (36.12 mg/kg), *Sambucus* (30.64 mg/kg), and *Salix* (21.26 mg/kg). The pronounced difference in total metal burden between *Laurus* and other species (2.3 to 3.3-fold higher)

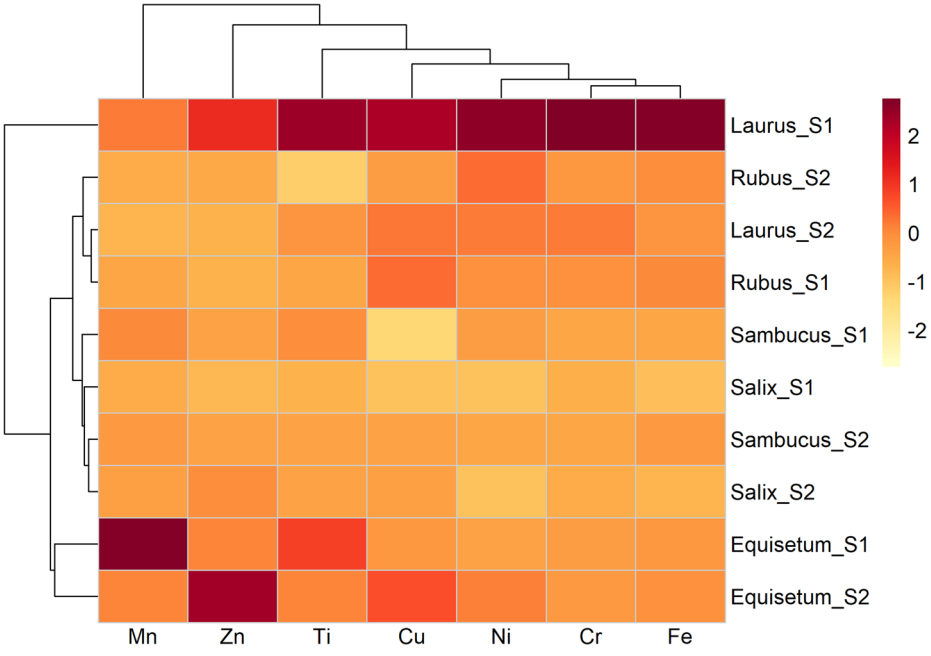

Fig. 3 Heatmap and hierarchical clustering of heavy metal concentrations (mg/kg) in riparian species from contaminated (S1) and reference (S2) sites. Colors represent normalized concentrations from low (yellow) to high (red)

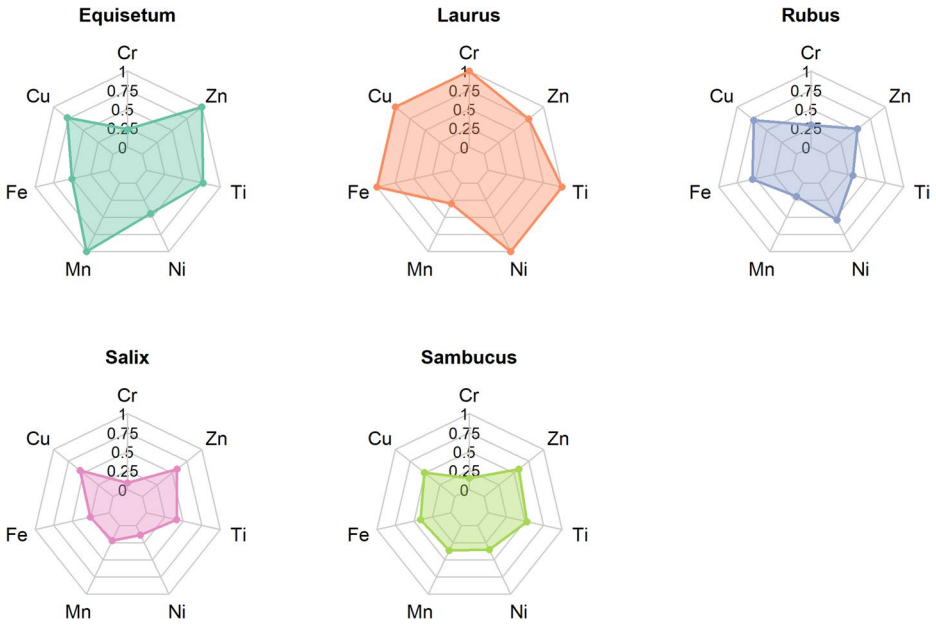

Fig. 4 Trace element concentrations in five plant species showing species-specific accumulation patterns

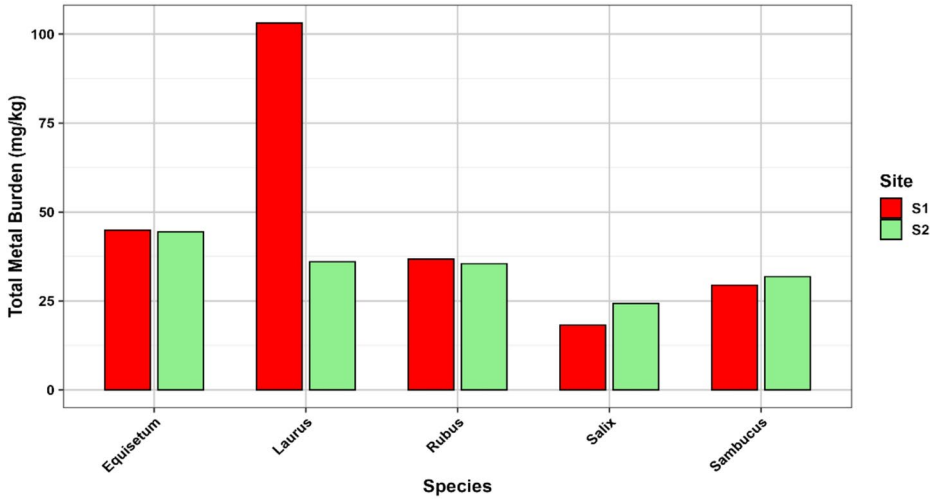

Fig. 5 Total metal burden in plant species at two sites (S1, S2)

indicated a fundamentally different physiological strategy for heavy metal handling. *Laurus* dominated sequestration for five of the seven heavy metals examined, achieving the highest leaf concentrations for Cr (9.42 mg/kg), Cu (0.98 mg/kg), Fe (42.55 mg/kg), Ni (3.93 mg/kg), and Ti (4.05 mg/kg), while *Equisetum* demonstrated preferential accumulation of Mn (6.59 mg/kg) and Zn (8.92 mg/kg). The radar plot analysis in (Fig. 4) shows these contrast-

ing accumulation profiles, with *Laurus* showing an expanded polygon encompassing multiple heavy metals, while other species displayed more selective patterns. The total metal burden comparison between sites (Fig. 5) revealed contrasting responses, with *Laurus* displaying the most dramatic site-specific difference (contaminated site burden of 103.13 mg/kg versus reference site values of 36.00 mg/kg), while *Equisetum*, *Rubus*, and *Sambucus* maintained relatively consistent total burdens between sites with ratios of 1.01, 1.04, and 0.93, respectively.

These findings have significant implications for phytoremediation applications and ecological risk assessment. The measured concentrations fell within expected ranges for contaminated vegetation, though Cr levels in *Laurus* approached potentially toxic thresholds (Al-Dahhan et al. 2024). The differential sequestration strategies observed likely reflect evolutionary adaptations to specific environmental conditions and phylogenetic constraints, with *Laurus* as a broadleaf evergreen shrub, possibly possessing enhanced vacuolar storage capacity and metallothionein production compared to herbaceous species (Qadir et al. 2021; Singha et al. 2025; Bhat et al. 2025). The pronounced Mn accumulation in *Equisetum* aligns with the known Mn tolerance of pteridophytes, possibly related to ancient detoxification pathways predating angiosperm evolution (Asare et al. 2025). *Laurus* emerges as a potential candidate for multi-metal phytoextraction, particularly for Cr and Fe, while *Equisetum* shows promise for Mn-specific remediation strategies. The consistent heavy metal burden patterns in some species suggest their utility as biomonitors for contamination assessment, while highly responsive species like *Laurus* indicate active hyperaccumulation strategies suitable for phytoremediation applications.

3.2 Contamination Gradients

Contamination factor (CF) reveals distinct heavy metals infiltration levels between industrial (S1) and reference (S2) sites, as shown in (Fig. 6), with three heavy metals showing high contamination levels ($CF > 3$), fourteen indicating moderate contamination (CF 1–3), and eighteen showing low contamination levels ($CF < 1$). Mn and Cr emerge as the primary pollutants, with *Laurus* showing the highest individual CF for Mn (4.84) and Cr (3.59), while *Equisetum* exhibits notable Mn contamination ($CF = 3.44$), indicating 3–5 times higher levels than background. Species-specific responses reveal distinct sensitivity patterns; *Laurus* demonstrates the strongest contamination response (mean $CF = 2.87$) with elevated values for six of seven heavy metals examined, while *Salix* exhibits the lowest response (mean $CF = 0.75$) with all metals in low contamination categories, suggesting enhanced exclusion mechanisms. *Rubus* shows moderate contamination for five heavy metals, with Ti highest ($CF = 2.47$), while *Sambucus* displays selective contamination for Mn ($CF = 1.42$), Ti ($CF = 1.29$), and Ni ($CF = 1.13$). Fe, despite being most abundant, shows modest CF values except in *Laurus* ($CF = 2.97$), while Cu and Zn display consistently low contamination factors across species.

The CF analysis signifies widespread contamination effects, with 48.6% of metal-species combinations showing $CF > 1.0$. High CF values for Mn and Cr suggest the most significant risk for phytotoxic effects and bioaccumulation. The species-specific variation demonstrates differential sensitivity with implications for ecological risk assessment, as *Laurus* may approach physiological stress thresholds while *Salix* maintains metal homeostasis despite elevated environmental concentrations. The contamination gradient pattern aligns with

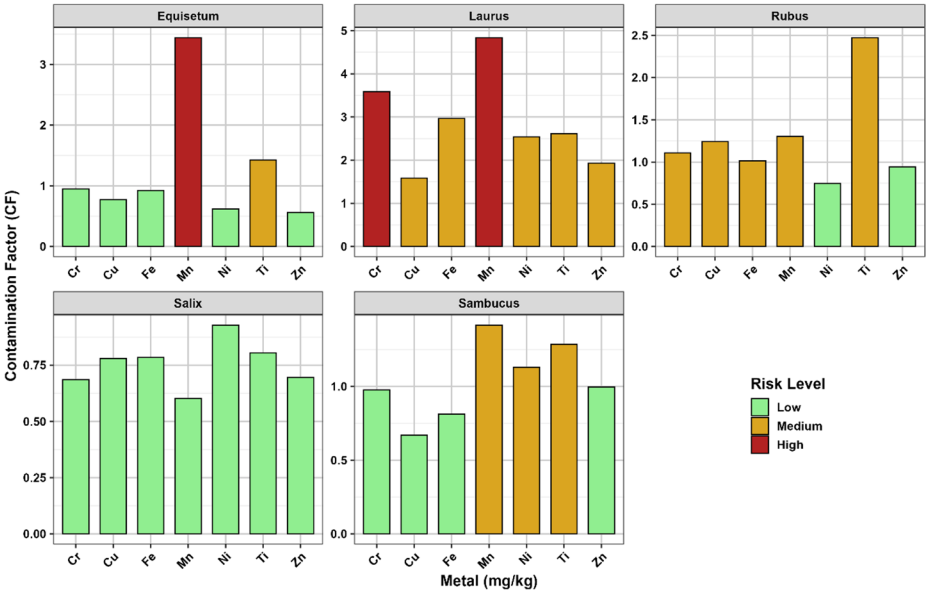

Fig. 6 Contamination factor (CF) for metals in five plant species showing risk levels (low, medium, high)

typical industrial pollution signatures, where specific heavy metals associated with manufacturing processes show pronounced enrichment relative to background levels (Kalozi et al. 2025; Reis et al. 2025; Zhou et al. 2025). The CF approach provides a standardized method for assessing contamination severity and comparing heavy metal accumulation patterns across different species and environmental contexts (Kang et al. 2023; Tamma et al. 2025). These results show significant contamination in the riparian ecosystem and support multi-species biomonitoring methods for a thorough assessment of contamination impacts (Kumar and Anshumali 2025; Tamma et al. 2025; Yan et al. 2025; Islamy et al. 2025).

3.3 Ecological Load of Heavy Metals

Comprehensive assessment of heavy metal contamination through integrated pollution and risk indices reveals significant variation in contamination severity and ecological risk across riparian plant species (Fig. 7). The Pollution Load Index (PLI) demonstrates that *Laurus* experiences the highest overall pollution burden (PLI = 2.67), falling within the heavy pollution category (PLI > 2), while *Equisetum* shows moderate pollution levels (PLI = 1.35). Three species display PLI values below unity, with *Rubus* (PLI = 1.01), *Sambucus* (PLI = 0.88), and *Salix* (PLI = 0.52) representing decreasing pollution load. The Ecological Risk Index (ERI) assessment reveals more pronounced risk differentials, with *Laurus* exhibiting the highest ecological risk (ERI = 47.59), approaching the moderate risk threshold (ERI = 40–80), while *Equisetum* demonstrates elevated risk levels (ERI = 20.16), and *Rubus*, *Sambucus*, and *Salix* show progressively lower risk indices (17.02, 12.97, and 7.99, respectively), all remaining within the low ecological risk category (ERI < 40).

Enrichment Factor (EF) analysis, using Fe as the reference element, effectively distinguishes anthropogenic metal sources from the natural geochemical background. Mn dem-

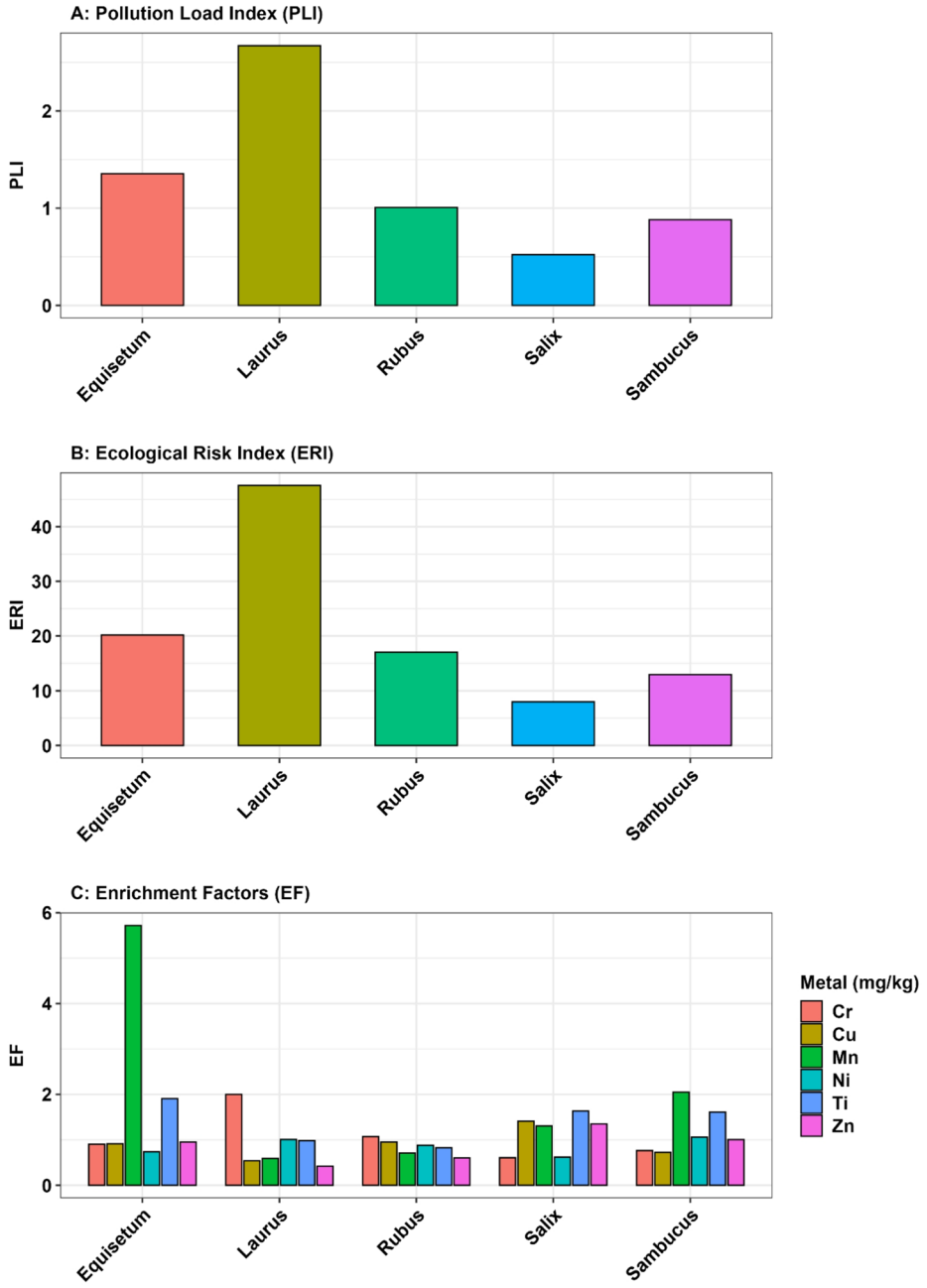

Fig. 7 Pollution indices in five plant species: (**A**) Pollution load index (PLI), (**B**) Ecological risk index (ERI), and (**C**) Enrichment factors (EF) for individual metals

onstrates the most significant anthropogenic enrichment, with *Equisetum* showing very high enrichment (EF = 5.72) and *Sambucus* displaying moderate enrichment (EF = 2.05), exceeding the threshold for moderate enrichment (EF > 2) and confirming anthropogenic Mn input. Cr shows the highest EF values in *Laurus* (EF = 1.99), approaching the moderate enrichment threshold, while Cu, Ni, Ti, and Zn generally exhibit EF values below 1.5 across all species, indicating limited anthropogenic influence. The selective enrichment of Mn and Cr supports their identification as primary contaminants of industrial origin within this riparian ecosystem. Species-specific pollution index patterns reflect differential physiological responses to multi-metal exposure, with *Laurus* consistently ranking highest across all three.

indices (PLI, ERI, EF composite), establishing this species as both the most contaminated and ecologically at risk, suggesting enhanced metal uptake mechanisms or a lack of effective exclusion strategies (Keshta et al. 2025; Al-Awah et al. 2026). Equally, *Salix* demonstrates the lowest pollution indices across all metrics, indicating effective heavy metal detoxification mechanisms or reduced bioavailability in its rhizosphere environment (Song et al. 2023; Vibhatabandhu et al. 2025). The integrated assessment reveals that current contamination may not pose immediate ecosystem-wide threats, but warrants continued monitoring (Majumdar et al. 2025; Nazir et al. 2025), while the EF analysis indicates Mn contamination is primarily anthropogenic in origin, supporting targeted remediation strategies focusing on Mn sources (Al-Awah et al. 2026).

3.4 Bioaccumulation Networks

Principal Component Analysis (PCA) reveals distinct co-accumulation patterns of metals in riparian plant leaf tissues, with the first two principal components explaining 86.5% of the total variance in metal concentrations (PC1: 68.8%, PC2: 17.7%), as shown in (Fig. 8A and B). The first principal component (PC1) is dominated by a strongly correlated group including Fe (loading = 0.972), Cr (0.956), Ni (0.942), and Cu (0.928), indicating synchronized accumulation mechanisms for these elements. This co-accumulation pattern likely reflects shared cellular transport systems, particularly the involvement of divalent metal transporter 1 (DMT1) and iron-regulated transporter (IRT) family proteins, which exhibit broad substrate specificity for Fe^{2+}, Cu^{2+}, Ni^{2+}, and other divalent cations (Aggarwal et al. 2025; Mishra et al. 2025; Liu et al. 2025b). Whereas the second principal component (PC2) is characterized by Mn as the dominant loading (0.927), with secondary associations for Ti (0.320) and Zn (0.359), indicating independent accumulation mechanisms. The distinct behavior of Mn reflects its specialized transport via NRAMP (Natural Resistance-Associated Macrophage Protein) family transporters and its essential role in photosynthetic oxygen evolution, requiring tight homeostatic regulation separate from other divalent metals (Mishra et al. 2025; Liu et al. 2025b).

Species groupings reveal distinct clustering patterns, with contaminated site (S1) samples showing considerable dispersion along PC1, *Laurus* S1 positioned at the extreme positive end (PC1 = 6.07), indicating exceptionally high concentrations of PC1-associated metals, and *Equisetum* S1 occupying a unique position (PC2 = 2.87), reflecting specialized Mn accumulation. Reference site (S2) demonstrates compact clustering with negative PC1 scores, with *Laurus* showing dramatic site-specific separation (S1: 6.07 vs. S2: −0.10), which signifies pronounced response to contamination gradients.

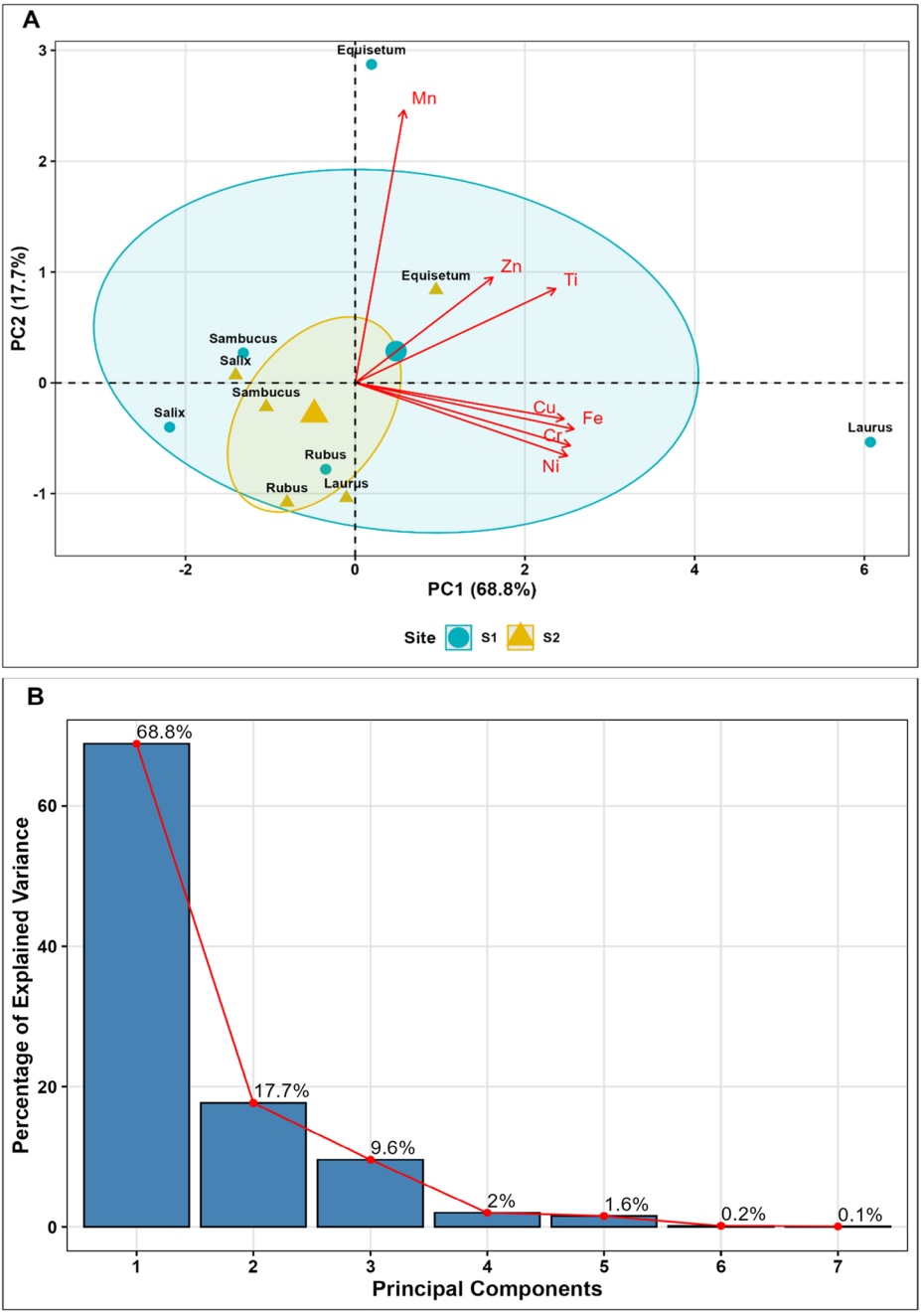

Fig. 8 Principal component analysis of metal concentrations: (**A**) biplot showing species distribution and metal loadings at two sites, (**B**) scree plot of explained variance

Spearman correlation analysis reveals complex metal interaction networks with distinct patterns between contaminated and reference sites (Fig. 9). Strong positive correlations dominate the overall dataset, with Fe-Cr emerging as the strongest relationship ($r = 0.93$, $p < 0.001$), followed by Cr-Ni ($r = 0.90$, $p < 0.001$), Fe-Ni ($r = 0.88$, $p < 0.01$), and Mn-Zn ($r = 0.89$, $p < 0.001$), establishing these as fundamental co-accumulation units. The contaminated site (S1) exhibits uniformly positive correlations, with several metal pairs achieving perfect correlation coefficients (Fe-Cr: $r = 1.00$; Ti-Zn: $r = 1.00$), suggesting overwhelmed cellular defense mechanisms where metals flood into cells through non-specific pathways when homeostatic capacity is exceeded, a phenomenon consistent with stress-induced breakdown of selective transport (El-Sappah et al. 2024; Mohamed et al. 2025a). While the reference site (S2) displays mixed correlation networks with both positive correlations (Cr-Ni: $r = 0.90$; Fe-Ni: $r = 0.90$; Mn-Zn: $r = 0.90$) and significant negative correlations (Cr-Zn: $r = -0.70$; Cu-Mn: $r = -0.60$; Ni-Zn: $r = -0.60$; Cr-Mn: $r = -0.60$), indicating competitive processes such as antagonistic interactions at membrane transporters and competition for binding sites on metallothioneins and phytochelatins (Nawaz et al. 2024; Acharya et al. 2025; Khan et al. 2025b).

The relationships between heavy metals reveal both complementary and independent accumulation strategies. The tight clustering of Fe, Cr, Ni, and Cu loadings on PC1 suggests shared cellular storage mechanisms, possibly involving vacuolar compartmentalization via tonoplast-localized transporters (VIT1, MTP family) or binding to metallothioneins and nicotianamine, which can chelate multiple divalent metals simultaneously (El-Sappah et al. 2024; Wang et al. 2025). On the other hand, Mn dominance in PC2 association and minimal PC1 loading (0.216) indicates distinct physiological handling consistent with its photosynthetic role and specialized transport systems (Wang et al. 2025). Negative correlations at the reference site indicate sophisticated regulatory mechanisms controlling metal homeostasis, with Cu-Mn ($r = -0.60$) and Cr-Zn ($r = -0.70$) antagonisms suggesting competitive binding or transport interference (Seregin et al. 2023; Rasheed et al. 2025; Mohamed et al. 2025b). The transformation from competitive to synergistic relationships between sites indicates contamination fundamentally alters plant physiology, shifting from selective uptake to bulk accumulation under stress (El-Sappah et al. 2024; Wang et al. 2025). Persistent correlations like Fe-Cr (All sites: $r = 0.93$; S1: $r = 1.00$; S2: $r = 0.70$) and Mn-Zn (All sites: $r = 0.89$; S1: $r = 0.90$; S2: $r = 0.90$) suggest fundamental storage mechanisms involving shared cellular compartments or binding molecules (El-Sappah et al. 2024; Wang et al. 2025).

The clear separation between PC1 and PC2 metal groups suggests contamination responses involve two independent physiological processes: a general heavy metal uptake system affecting Fe, Cr, Ni, and Cu simultaneously, and a specialized Mn transport system operating independently. Species like *Laurus* demonstrate capacity for multi-metal accumulation, while *Equisetum* shows selectivity for Mn extraction (Wu et al. 2024; Peralbo et al. 2025). The scree plot analysis in (Fig. 8B) indicates the first two components capture essential dimensionality (<10% variance in subsequent components), validating that riparian plant metal accumulation operates through two primary axes representing distinct contamination processes. These patterns have significant implications for phytoremediation applications: enhanced positive correlations under contaminated conditions support multi-metal phytoextraction approaches, while competitive relationships under reference conditions favor targeted single-metal remediation strategies. These findings provide a foundation for developing species-specific biomonitoring strategies and optimizing phytoremediation

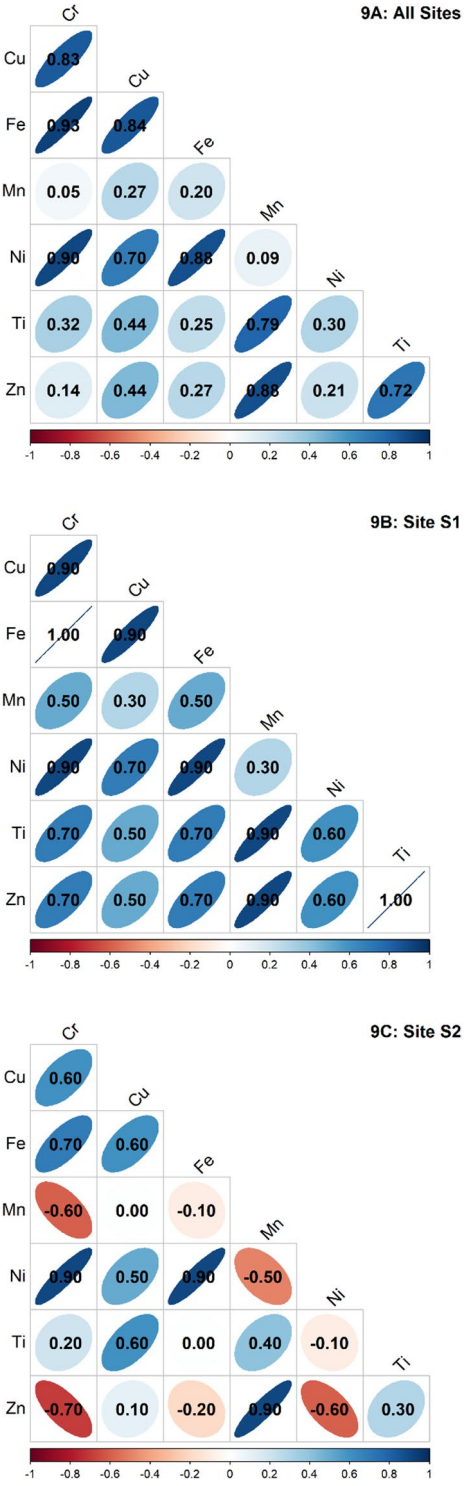

Fig. 9 Correlation matrices of metal concentrations: (**A**) all sites combined, (**B**) site S1, and (**C**) site S2

approaches based on metal-specific accumulation affinities (Ogwu et al. 2025b; Gampson et al. 2025).

3.5 Biogeochemical Indicators

Essential heavy metal relationship reveals critical insights into biogeochemical balance disruption in riparian plant leaf tissues, with Fe-Zn and Cu-Mn ratios serving as sensitive indicators of contamination-induced physiological stress (Fig. 10). The Fe-Zn relationship analysis demonstrates pronounced species-specific contamination responses, with *Laurus* exhibiting the most dramatic deviation from normal biogeochemical balance. Under reference conditions, the Fe/Zn ratio in *Laurus* maintains relatively stable relationships (Fe/Zn≈4.7), consistent with normal cellular Fe storage and Zn transport mechanisms. However, at the contaminated site, this ratio increases dramatically to 7.3, indicating preferential Fe accumulation and potential disruption of Zn homeostasis mechanisms through competitive inhibition at cellular binding sites (Shiryaev et al. 2024; Kumar and Anshumali 2025; Singha et al. 2025). *Equisetum* exhibits remarkable biogeochemical stability with ratios remaining relatively constant (S1: 3.2; S2: 1.9), indicating robust homeostatic mechanisms possibly reflecting evolutionary adaptations to variable metal environments. *Salix*, *Rubus*, and *Sambucus* show intermediate responses with moderate Fe-Zn ratio alterations, suggesting varying degrees of biogeochemical sensitivity among woody riparian species (Shiryaev et al. 2024; Kumar and Anshumali 2025; Singha et al. 2025).

Cu-Mn concentration patterns reveal differential biogeochemical sensitivity among species, with *Laurus* experiencing the most severe disruption as Cu/Mn ratios shift from 1.12 at the reference site to 0.37 at the contaminated site. This dramatic decrease suggests Mn

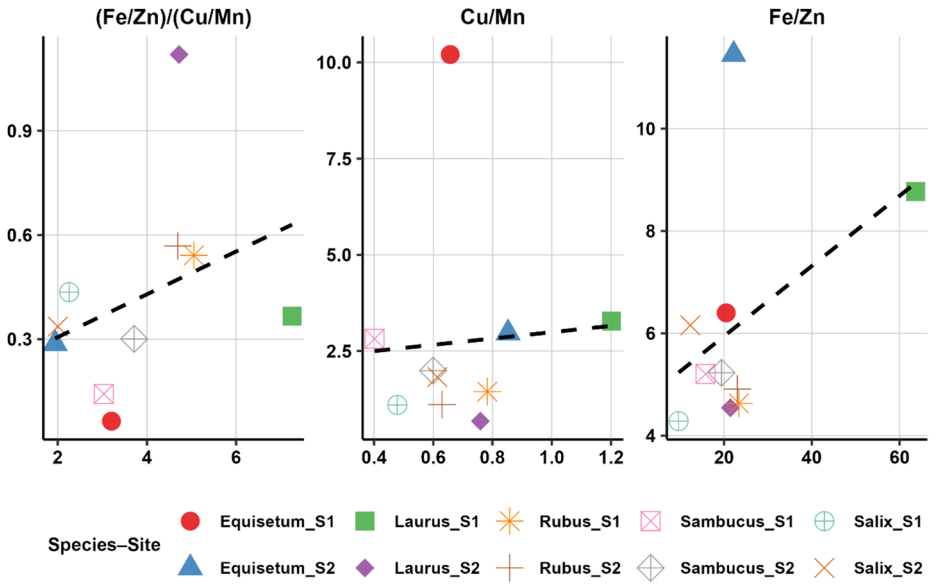

Fig. 10 Metal ratio relationships across plant species and sites showing correlations between Fe/Zn, Cu/Mn, and combined ratios

accumulation overwhelms Cu homeostasis, potentially disrupting photosynthetic electron transport chains and oxidative stress defense mechanisms, indicating *Laurus* approaches critical biogeochemical thresholds where essential metal balance becomes severely compromised (Tang et al. 2024; Bai et al. 2025). *Equisetum* displays different Cu-Mn relationship patterns, maintaining relatively stable ratios across sites (S1: 0.064; S2: 0.287) with consistently lower values reflecting its specialized Mn accumulation strategy. This suggests pteridophyte species possess distinct biogeochemical regulation mechanisms accommodating high Mn concentrations without proportional disruption of Cu-dependent processes, potentially through primitive but effective homeostatic mechanisms conferred by evolutionary antiquity (Hossain et al. 2022; Jungová et al. 2022).

Integrated ratio analysis (Fe/Zn vs. Cu/Mn) provides comprehensive biogeochemical fingerprinting for enhanced contamination detection, revealing species-specific clustering patterns in multidimensional biogeochemical space. Reference site samples cluster within a defined biogeochemical envelope, indicating normal metal homeostasis, while contaminated site samples show pronounced dispersion, with *Laurus* exhibiting the significant deviation, positioned at extreme coordinates reflecting both elevated Fe/Zn and depressed Cu/Mn ratios (Liang et al. 2025; Nechita et al. 2025; Kumar and Anshumali 2025).

Species clustering patterns reveal distinct homeostatic strategies: *Salix* and *Sambucus* form tight clusters in both conditions, suggesting similar biogeochemical regulation mechanisms, *Rubus* occupies intermediate positions, while *Equisetum* and *Laurus* represent biogeochemical extremes reflecting divergent approaches to metal accumulation and homeostasis (Kalozi et al. 2025; Nasca et al. 2025). Trend line slopes serve as quantitative indicators of biogeochemical disruption magnitude, with reference site data exhibiting positive correlation (slope$\approx$0.85) indicating coordinated regulation under normal conditions, while contaminated site data shows steep negative correlation (slope ≈ -1.45) reflecting dysregulation where Fe accumulation correlates with Mn excess and Cu depletion (Shukla et al. 2024). The slope change magnitude (Δslope $= -2.30$) provides quantitative measures of ecosystem-wide biogeochemical disruption. Biogeochemical balance maintenance capabilities vary dramatically among species, with implications for ecosystem resilience and restoration potential. *Equisetum* demonstrates superior stability, maintaining essential metal ratios within acceptable ranges despite elevated environmental metal concentrations, suggesting pteridophyte species may serve as biogeochemical stabilizers in contaminated riparian systems, potentially facilitating ecosystem recovery through maintenance of normal nutrient cycling processes (Hassan et al. 2024; Nasca et al. 2025). Spatial biogeochemical gradient patterns indicate contamination effects extending beyond simple metal accumulation to encompass fundamental disruption of plant nutritional physiology, with systematic deviation from reference conditions across all species suggesting ecosystem-wide perturbations in essential metal relationships. These biogeochemical indicators offer valuable tools for environmental assessment, providing quantitative measures extending beyond simple concentration measurements, with species-specific response patterns supporting the development of multi-species biomonitoring approaches detecting biogeochemical disruption at multiple scales of biological organization (Hassan et al. 2024; Shiryaev et al. 2024; Shukla et al. 2024; Nechita et al. 2025; Kalozi et al. 2025; Nasca et al. 2025).

3.6 Sustainable Phytoremediation Applications

Phytoremediation using riparian vegetation offers significant potential for mitigating heavy metal contamination while contributing to the United Nations Sustainable Development Goals (SDGs). In this study, *Laurus* exhibited the highest Pollution Load Index (PLI = 2.67), with substantial accumulation of Fe and Cr. This aligns with reports indicating its biosorption capacity for Cd, Pb, Cu, and Zn in aqueous and terrestrial environments (Rai and Nongtri 2024; Nasca et al. 2025). Similarly, *Equisetum* has been documented as an effective accumulator of Mn and Zn, supported by its silica-rich tissues that enhance rhizofiltration processes in wetlands and mining-affected soils (López Rodríguez et al. 2021; PANIZZA 2025). These findings suggest that both species are suitable for targeted remediation depending on site-specific pollutants.

Other species contribute to ecological stability and restoration. *Rubus* and *Sambucus* have been identified as useful hedgerow components in ecological restoration systems, where they function as stabilizers and moderate bioaccumulators of Zn, Pb, Cd, and Cu (PANIZZA 2025; Nasca et al. 2025). Their role supports SDG 15 (Life on Land) through soil quality improvement and habitat restoration, and *Sambucus* additionally contributes to SDG 11 (Sustainable Cities and Communities) by lowering human exposure to contaminated soils in peri-urban environments.

Salix remains a key species for dendroremediation due to its high biomass production, deep-rooted system, and proven ability to accumulate Pb, Cd, and Zn in riparian environments. Reports emphasize its consistent role in pollutant removal and ecological restoration, highlighting its importance in long-term, large-scale projects (Khan et al. 2025a; Najwa et al. 2025). Its applications contribute to SDG 6 (Clean Water), SDG 13 (Climate Action), SDG 15 (Life on Land), and SDG 17 (Partnerships for the Goals), demonstrating the integrative role of dendroremediation in sustainable landscape management.

4 Conclusions

This study introduces a new approach in monitoring Mediterranean riparian ecosystems by showing that native plant communities act as advanced biological sensors capable of detecting and measuring industrial pollution with exceptional accuracy. The successful validation of TXRF spectroscopy as a better analytical method than conventional ICP-AOS techniques marks a significant breakthrough, providing increased sensitivity and better tolerance for complex matrices that will transform trace element analysis in environmental biomonitoring efforts worldwide. The discovery of species-specific metal accumulation patterns, with *Laurus* emerging as a notable multi-metal hyperaccumulator and *Equisetum arvense* showing specialized Mn sequestration, provides the scientific basis for creating targeted, sustainable cleanup strategies aligned with circular economy principles. These results go beyond academic interest by offering practical solutions to one of Europe's biggest environmental challenges: restoring industrially affected watersheds that supply millions of residents. The biogeochemical disruption patterns uncovered through innovative ratio analyses offer early warning signs of ecosystem stress, allowing for proactive intervention before irreversible damage happens. This predictive ability is vital for safeguarding biodiversity hotspots like the Mediterranean basin, where climate change increases contamination risks through

altered rainfall patterns and extreme weather events. By integrating advanced analytical chemistry with ecological restoration, this study demonstrates how phytoremediation can contribute to multiple UN Sustainable Development Goals. The identified approaches offer cost-effective, nature-based solutions that enhance water security, protect terrestrial ecosystems, and promote sustainable urban development, while supporting both ecological recovery and economic growth in post-industrial landscapes.

Acknowledgements This study acknowledges the DiSPUTer, Department of Psychological Health and Territory Sciences, and DATA – U.D'A Analytical High-Tech Laboratory. The authors thank Prof. Laura Borgese for her scientific support in improving our TXRF expertise and enabling the UdA research team to participate in the Enforce TXRF COST Action no. 18130.

Author Contributions S.A.T. contributed to sample collection, preparation, analysis, data validation, and visualization, and drafted the manuscript. S.C.D.S. contributed to sample preparation and analysis. A.A., H.A and M.Y.J.B assisted with data analysis. F.S. provided co-supervision. L.M. was involved in sample collection, preparation, and analysis. B.M.S.G. assisted with quality improvement. G.R. served as the primary supervisor, conceptualized the research, secured funding, and participated in sample collection, analysis, data validation, quality assurance, and data management. All authors reviewed the manuscript.

Funding Open access funding provided by Università degli Studi G. D'Annunzio Chieti Pescara within the CRUI-CARE Agreement. Financial support for this research was provided by the DiSPUTer, Department of Psychological Health and Territory Sciences, and the DATA – U.D'A Analytical High-Tech Laboratory located at the "G. d'Annunzio" University in Chieti, Italy (66100).

Data Availability Data will be available on request.

Declarations

Competing interests The authors declare no competing interests.

References

Acharya A, Bellaloui N, Pilipovic A et al (2025) Current assessment and future perspectives on phytoremediation of heavy metals. Plants 14. https://doi.org/10.3390/plants14182847

Aggarwal M, Anbukumar S, Kumar TV (2025) The relationship between pH, organic matter and heavy metal concentrations in surface sediment of Ganga River, India. Water Environ Res 97:e70160. https://doi.org/10.1002/wer.70160

Al-Awah H, Radwan AE, El-Sorogy AS (2026) Integrated risk assessment of heavy metals in marine sediments from Salwa Bay, Qatar using pollution indices and multivariate analysis. Mar Pollut Bull 222:118903. https://doi.org/10.1016/j.marpolbul.2025.118903

Al-Dahhan WH, Ali MA, Hasan AA et al (2024) Heavy metals detection in some types of herbs used in medical treatments. Al-Kitab Journal for Pure Sciences 8:71–80. https://doi.org/10.32441/kjps.08.01.p7

Alvarez X, Rivas P, Acña-Alonso C, Valero E (2021) Evaluation and analysis of riparian vegetation through satellite images. https://meetingorganizer.copernicus.org/EGU21/EGU21-7306.html. Accessed 9 Aug 2025

Andersone-Ozola U, Jēkabsone A, Karlsons A et al (2025) Heavy metal tolerance and accumulation potential of a rare coastal Species, anthyllis vulneraria subsp. Maritima. Stresses 5. https://doi.org/10.3390/stresses5010006

Asare MO, Pellegrini E, Száková J et al (2025) Abilities of herbaceous plant species to phytoextract Cd, Pb, and Zn from arable soils after poly-metallic mining and smelting. Environ Sci Pollut Res 32:8834–8849. https://doi.org/10.1007/s11356-025-36241-6

Bai X, Wu S, Bai A-N et al (2025) OsSPL9 promotes Cu uptake and translocation in rice grown in high-Fe red soil. New Phytol 246:2207–2221. https://doi.org/10.1111/nph.70074

Baloch MYJ, Talpur SA, Talpur HA et al (2020) Effects of arsenic toxicity on the environment and its remediation techniques: a review. J Water Environ Technol 18:275–289. https://doi.org/10.2965/jwet.19-130

Baloch MYJ, Zhang W, Chai J et al (2025) Groundwater contamination, fate, and transport of fluoride and nitrate in Western Jilin, china: implications for water quality and health risks. Environ Chem Ecotoxicol. https://doi.org/10.1016/j.enceco.2025.04.010

Bellino A, Alfani A, De Riso L et al (2020) A promising cosmopolitan biomonitor of potentially toxic elements in freshwater ecosystems: concentration gradients in sensitive areas. Ecol Ind 109:105801. https://doi.org/10.1016/j.ecolind.2019.105801

Bessonova V, Sklyarenko A (2020) Dynamics of chlorine content in leaves of woody plants of protection forest bands in the city of Zaporizhzhya. Ekológia (Bratislava) 39:214–223. https://doi.org/10.2478/eko-2020-0016

Bhat BA, Rather MA, Bilal T et al (2025) Plant hyperaccumulators: a state-of-the-art review on mechanism of heavy metal transport and sequestration. Front Plant Sci 16. https://doi.org/10.3389/fpls.2025.1631378

Cakaj A, Drzewiecka K, Hanć A et al (2024) Plants as effective bioindicators for heavy metal pollution monitoring. Environ Res 256:119222. https://doi.org/10.1016/j.envres.2024.119222

Castellani F, Manzoli L, Martellucci CA et al (2021) Levels of polychlorinated dibenzo-*p*-dioxins/furans and polychlorinated biphenyls in free-range hen eggs in central Italy and estimated human dietary exposure. J Food Prot 84:1455–1462. https://doi.org/10.4315/JFP-21-126

Dinca L, Murariu G, Lupoae M (2025) Understanding the ecosystem services of riparian forests: patterns, gaps, and global trends. Forests 16:947. https://doi.org/10.3390/f16060947

Dodds WK, Barmuta LA, Bernal S et al (2025) Defining stream riparian zones across multidimensional environmental gradients. J Environ Qual 54:1674–1697. https://doi.org/10.1002/jeq2.70080

El-Sappah AH, Zhu Y, Huang Q et al (2024) Plants' molecular behavior to heavy metals: from criticality to toxicity. Front Plant Sci 15. https://doi.org/10.3389/fpls.2024.1423625

Gampson EK, Dodd M, d'Entremont MV (2025) Source and distribution of heavy metals in sediment samples from select creeks of the highly urbanized metro Vancouver watersheds, Canada. Discov Environ 3:35. https://doi.org/10.1007/s44274-025-00220-y

Gong B, He E, Qiu H et al (2020) Interactions of arsenic, copper, and zinc in soil-plant system: Partition, uptake and phytotoxicity. Sci Total Environ 745:140926. https://doi.org/10.1016/j.scitotenv.2020.140926

Hassan J, Rajib MMR, Khan MdN-E-A et al (2024) Assessment of heavy metals accumulation by vegetables irrigated with different stages of textile wastewater for evaluation of food and health risk. J Environ Manage 353:120206. https://doi.org/10.1016/j.jenvman.2024.120206

Haydous F, Nehmeh B, Rebehmed J et al (2025) Unraveling the levels of emerging contaminants along the Eastern mediterranean sea. Sci Rep 15:4401. https://doi.org/10.1038/s41598-025-89027-8

Heta G, Zejnullahu F, Zeneli V et al (2025) Ecological risk factor, contamination factor and bioconcentration factor of heavy metals in vegetables grown on polluted soils in Kosovo. Pol J Environ Stud. https://doi.org/10.15244/pjoes/209221

Hossain MB, Masum Z, Rahman MS et al (2022) Heavy metal accumulation and phytoremediation potentiality of some selected Mangrove species from the world's largest Mangrove forest. Biology 11:1144. https://doi.org/10.3390/biology11081144

Intergovernmental Panel On Climate Change (Ipcc) (2023) Climate change 2022 – Impacts, adaptation and vulnerability: working group II contribution to the sixth assessment report of the intergovernmental panel on climate change, 1st edn. Cambridge University Press

Iqbal J, Su C, Rashid A et al (2021) Hydrogeochemical assessment of groundwater and suitability analysis for domestic and agricultural utility in Southern Punjab. Pakistan Water 13:3589. https://doi.org/10.3390/w13243589

Islamy RA, Hasan V, Kamarudin AS et al (2025) Biomonitoring of heavy metal pollution in the Brantas River using genotoxic and histopathological biomarkers in wild cyprinidae. J Ecol Eng 26:1–11. https://doi.org/10.12911/22998993/206050

Jat Baloch MY, Zhang W, Chai J et al (2021) Shallow groundwater quality assessment and its suitability analysis for drinking and irrigation purposes. Water 13:3361. https://doi.org/10.3390/w13233361

Jat Baloch MY, Su C, Talpur SA et al (2023) Arsenic removal from groundwater using iron pyrite: influence factors and removal mechanism. J Earth Sci 34:857–867. https://doi.org/10.1007/s12583-022-1698-x

Jungová M, Asare MO, Jurasová V, Hejcman M (2022) Distribution of micro- (Fe, Zn, Cu, and Mn) and risk (Al, As, Cr, Ni, Pb, and Cd) elements in the organs of *Rumex alpinus* L. in the Alps and Krkonoše Mountains. Plant Soil 477:553–575. https://doi.org/10.1007/s11104-022-05440-2

Kalozi O, Kebert M, Orlović S et al (2025) Populus × Euramericana accumulates more organic pollutants (PAHs and PCBs), while P. nigra 'Italica' absorbs more heavy metals. Plants 14. https://doi.org/10.3390/plants14101445

Kang Y, Zheng S, Wan T et al (2023) Nematode as a biomonitoring model for evaluating ecological risks of heavy metals in sediments from an urban river. Ecol Ind 147:110013. https://doi.org/10.1016/j.ecolind.2023.110013

Kawałko D, Karczewska A, Lewińska K (2023) Environmental risk associated with accumulation of toxic metalloids in soils of the Odra river floodplain—case study of the assessment based on total concentrations, fractionation and geochemical indices. Environ Geochem Health 45:4461–4476. https://doi.org/10.1007/s10653-023-01502-1

Keshta AE, Gagnon JE, Barrette J, Shaheen ME (2025) Pollution load index and ecological risk assessment of sediment heavy metals in lake Edku, Egypt. Bull Environ Contam Toxicol 114:84. https://doi.org/10.1007/s00128-025-04054-5

Khan AHA, Budzyńska S, Zine H et al (2025a) Dendroremediation: A sustainable nature-based solution for management of abandoned mining sites and brownfields. J Clean Prod 501:145342. https://doi.org/10.1016/j.jclepro.2025.145342

Khan T, Shah L, Khan S et al (2025b) Comprehensive review of multiomics applications and remediation of plant heavy metal toxicity. Stress Biology 5:58. https://doi.org/10.1007/s44154-025-00233-w

Koç İ, Canturk U, Isinkaralar K et al (2024) Assessment of metals (Ni, Ba) deposition in plant types and their organs at Mersin City, Türkiye. Environ Monit Assess 196:282. https://doi.org/10.1007/s10661-024-12448-x

Kumar S, Anshumali (2025) Heavy metal pollution and health risk assessment in upland and riparian soils of the Ganga river basin. Discov Soil 2:33. https://doi.org/10.1007/s44378-025-00061-4

Leibowitz SG, Hill RA, Creed IF et al (2023) National hydrologic connectivity classification links wetlands with stream water quality. Nat Water 1:370–380. https://doi.org/10.1038/s44221-023-00057-w

Liang X, Zhang X, Li Y et al (2025) Genome-Wide identification of heavy metal ATPase family in Aegilops Tauschii and functional verification of AetHMA4 and AetHMA8. Agronomy 15. https://doi.org/10.3390/agronomy15030714

Lin T, Manan A, Yang S et al (2025) Heavy metal pollution enhances pathogen resistance of an invasive plant species over its native congener. Funct Ecol 39:1096–1111. https://doi.org/10.1111/1365-2435.70011

Liu H, Li C, Fan Z et al (2025a) Synergistic enhancement of Cobalt adsorption by graphitization and magnetic modification of biochar: Synthesis, Characterization, performance and mechanism. Water Air Soil Pollut 236:929. https://doi.org/10.1007/s11270-025-08570-2

Liu W, Zhou A, Shao Z et al (2025b) Genome annotation of Molting-Related Protein-Coding genes in propsilocerus Akamusi reveals transcriptomic responses to heavy metal contamination. Insects 16. https://doi.org/10.3390/insects16060636

López Rodríguez CC, Izquierdo Ramírez CR, Lanfranco Colina LJ et al (2021) Phytoextraction of Heavy Metals from the Soil of Aurora-Patricia Mining Environmental Liability by Herbaceous Species Carex mandoniana, Equisetum bogotense, and Muehlenbeckia tamnifolia, La Encañada-Peru 2020. In: Iano Y, Saotome O, Kemper G,. (eds) Proceedings of the 6th Brazilian Technology Symposium (BTSym'20). Springer International Publishing, Cham, pp 100–109

Maeyouf H, Khattab RA, Temraz T et al (2025) Heavy metal contamination in seawater, sediments, algae, and fish from Susah and Tobruk, mediterranean sea. Water Environ Res 97:e70091. https://doi.org/10.1002/wer.70091

Majumdar A, Avishek K, Finger DC (2025) Riparian soil heavy metal contamination and pollution assessment and management planning integrating multiple indices, statistical and geospatial approaches. Environ Manage 75:402–423. https://doi.org/10.1007/s00267-025-02112-6

Mishra A, Bhat A, Kumari S et al (2025) Time-series multi-omics analysis of micronutrient stress in *Sorghum bicolor* reveals iron and zinc crosstalk and regulatory network conservation. Plant Biol J Plb 70038. https://doi.org/10.1111/plb.70038

Mohamed HI, Ullah I, Toor MD et al (2025a) Heavy metals toxicity in plants: Understanding mechanisms and developing coping strategies for remediation: a review. Bioresour Bioprocess 12:95. https://doi.org/10.1186/s40643-025-00930-4

Mohamed HI, Ullah I, Toor MD et al (2025b) Heavy metals toxicity in plants: Understanding mechanisms and developing coping strategies for remediation: a review. Bioresour Bioprocess 12:95. https://doi.org/10.1186/s40643-025-00930-4
Najwa N, Abdullah S, Mohd Noor NA (2025) Phytoremediation as a sustainable approach for heavy metal removal from wastewater: insights from Salvinia molesta, pistia stratiotes, and lemnoideae studies. IOP Conf Ser: Earth Environ Sci 1548:012029. https://doi.org/10.1088/1755-1315/1548/1/012029
Nasca O, Dippong T, Resz M-A et al (2025) Interdisciplinary evaluation of the Săpânța river and groundwater quality: linking hydrological data and vegetative bioindicators. Water 17. https://doi.org/10.3390/w17131975
Natasha, Shahid M, Khalid S et al (2020) A critical review of mercury speciation, bioavailability, toxicity and detoxification in soil-plant environment: ecotoxicology and health risk assessment. Sci Total Environ 711:134749. https://doi.org/10.1016/j.scitotenv.2019.134749
Nawaz A, Šotek PE, Molnárová M (2024) Reciprocal effects of metal mixtures on phytoplankton. Phycology 4:117–138. https://doi.org/10.3390/phycology4010007
Nazir A, Riyaz M, Zargar MA, Afzal M (2025) Spatial distribution, sources, ecological risk assessment of heavy metals in surface sediments of Wular lake, Kashmir, India-a Ramsar site. Front Environ Sci 13. https://doi.org/10.3389/fenvs.2025.1630494
Nechita C, Iordache AM, Roba C et al (2025) Heavy metal health risk assessment in Picea abies L. Forests along an altitudinal gradient in Southern Romania. Plants 14. https://doi.org/10.3390/plants14060968
Neumann M, Jáchymová B, Koudelka P et al (2025) Mobility of sediment and phosphorus in a small stream during artificial flood wave. Environ Process 12:3. https://doi.org/10.1007/s40710-025-00744-8
Ogwu MC, Izah SC, Sawyer WE, Amabie T (2025a) Environmental risk assessment of trace metal pollution: A statistical perspective. Environ Geochem Health 47:94. https://doi.org/10.1007/s10653-025-02405-z
Ogwu MC, Izah SC, Sawyer WE, Amabie T (2025b) Environmental risk assessment of trace metal pollution: A statistical perspective. Environ Geochem Health 47:94. https://doi.org/10.1007/s10653-025-02405-z
Palma P, Fialho S, Lima A et al (2021) Occurrence and risk assessment of pesticides in a mediterranean basin with strong agricultural pressure (Guadiana basin: Southern of Portugal). Sci Total Environ 794:148703. https://doi.org/10.1016/j.scitotenv.2021.148703
PANIZZA A (2025) Le migliori pratiche gestionali per la conservazione della natura e la produttività: il caso studio di Marsilea quadrifolia L. in prati umidi
Papazoglou EG, Zine H, Trigas P et al (2025) Native plant responses and elemental accumulation in mining and metallurgical mediterranean ecosystems. Plants 14. https://doi.org/10.3390/plants14172646
Peralbo JIB, Peco J, Villena J et al (2025) Transference of potentially toxic elements from soils to plants in a derelict Pb-Zn mining area (San Quintín mine, South-Central Spain)
Popa G, Mihăiescu TC, Odagiu A, IN RIPARIAN VEGETATION IN BAIUT METALLOGENIC AREA, MARAMURES COUNTY (ROMANIA) (2019) HEAVY METALS ACCUMULATION. Studia Universitatis Babeș-Bolyai Chem 457–469. https://doi.org/10.24193/subbchem.2019.2.39
Qadir SU, Raja V, Siddiqi WA et al (2021) Heavy metal bioaccumulation by selected plants from fly ash–contaminated soils in suburban area. Arab J Geosci 14:116. https://doi.org/10.1007/s12517-020-06445-w
Rai PK, Nongtri ES (2024) Heavy metals/-metalloids (As) phytoremediation with *Landoltia punctata* and *lemna* sp. (duckweeds): coupling with biorefinery prospects for sustainable phytotechnologies. Environ Sci Pollut Res 31:16216–16240. https://doi.org/10.1007/s11356-024-32177-5
Rasheed YS, AL-Janaby MS, Abbas MH (2025) Identification and functional annotation of echium plantagineum Metallothioneins for reduction in heavy metals in soil using molecular Docking. Nat Env Poll Tech 24:D1671. https://doi.org/10.46488/NEPT.2025.v24i01.D1671
Rawat H, Bhat SA, Dhanjal DS et al (2024) Emerging techniques for the trace elemental analysis of plants and food-based extracts: A comprehensive review. Talanta Open 10:100341. https://doi.org/10.1016/j.talo.2024.100341
Reis GA, Alves Martins MV, Santos LMG et al (2025) Contamination by Potentially Toxic Elements (PTEs) in Agricultural Products Grown Around Sepetiba Bay, Rio de Janeiro State (SE Brazil). Arch Environ Contam Toxicol 89:195–220. https://doi.org/10.1007/s00244-025-01143-8
Seregin IV, Kozhevnikova AD, Seregin IV, Kozhevnikova AD (2023) Nicotianamine: A key player in metal homeostasis and hyperaccumulation in plants. Int J Mol Sci 24. https://doi.org/10.3390/ijms241310822
Shiryaev G, Maleva M, Borisova G et al (2024) Phytomitigation potential and adaptive responses of helophyte typha latifolia L. to copper smelter-influenced heavily multi-metal contamination. Environ Sci Pollut Res 31:38821–38834. https://doi.org/10.1007/s11356-023-25973-y
Shtull-Trauring E, Egozi R, Ben-Yona M, Bernstein N (2025) Insights from intensive stream monitoring in an Eastern mediterranean agricultural catchment illuminate anthropogenic impact on water quality. River Res Appl 41:138–151. https://doi.org/10.1002/rra.4380

Shukla AK, Behera SK, Basumatary A PCA and fuzzy clustering-based delineation of soil nutrient (S, Zn B et al (2024) Mn, Fe, and Cu) management zones of sub-tropical Northeastern India for precision nutrient management. Journal of Environmental Management 365:121511. https://doi.org/10.1016/j.jenvman.2024.121511

Singha L, Singh RSJ, Priyadharshini B et al (2025) Heavy metal stress in plants: Mechanisms, Impacts, and mitigation Strategies- A comprehensive review. Int J Environ Sci 2968–2977. https://doi.org/10.64252/yjv3t467

Song H, Kuang L, Wang L et al (2023) Potential ecological risks of heavy metals and Cd accumulation characteristics of *Suaeda salsa* under different Cd input and water logging conditions in the Yellow River estuary, China. Environ Sci Pollut Res 30:85170–85183. https://doi.org/10.1007/s11356-023-28373-4

Talpur SA, Noonari TM, Rashid A et al (2020) Hydrogeochemical signatures and suitability assessment of groundwater with elevated fluoride in unconfined aquifers badin district, Sindh, Pakistan. SN Appl Sci 2:1038. https://doi.org/10.1007/s42452-020-2821-1

Talpur HA, Talpur SA, Mahar A et al (2024) Investigating drinking water quality, microbial pollution, and potential health risks in selected schools of Badin city, Pakistan. HydroResearch 7:248–256. https://doi.org/10.1016/j.hydres.2024.04.004

Talpur SA, Cinosi A, Stoppa F et al (2025a) Heavy metals pollution of Pescara river (southern Italy): risk assessment based on total reflection X-ray fluorescence analyses. Mar Pollut Bull 211:117397. https://doi.org/10.1016/j.marpolbul.2024.117397

Talpur SA, Rashad M, Ahmed A et al (2025b) Pollution indicators and human health risk assessment of fluoride contaminated drinking groundwater in southern Pakistan. HydroResearch 8:167–177. https://doi.org/10.1016/j.hydres.2024.10.005

Tamma AA, Lejcuś K, Fiałkiewicz W et al (2025) Advancing phytoremediation: A review of soil amendments for heavy metal contamination management. Sustainability 17. https://doi.org/10.3390/su17135688

Tang Z, Li Y-F, Zhang Z-H et al (2024) OsCOPT7 is a copper exporter at the tonoplast and endoplasmic reticulum and controls Cu translocation to the shoots and grain of rice. Plant Cell Environ 47:2163–2177. https://doi.org/10.1111/pce.14867

Tarish M, Ali RT, Shan M et al (2024) Plant tissues as biomonitoring tools for environmental contaminants. Int J Plant Biol 15:375–396. https://doi.org/10.3390/ijpb15020030

Tőzsér D, Horváth R, Simon E, Magura T (2023) Heavy metal uptake by plant parts of Populus species: a meta-analysis. Environ Sci Pollut Res 30:69416–69430. https://doi.org/10.1007/s11356-023-27244-2

Vibhatabandhu P, Leelakun P, Yottiam A et al (2025) Integration of microplastics and heavy metals in the potential ecological risk index: Spatial pollution assessment of sediments in the inner Gulf of Thailand. Chemosphere 376:144280. https://doi.org/10.1016/j.chemosphere.2025.144280

Vitali M, Castellani F, Fragassi G et al (2021) Environmental status of an Italian site highly polluted by illegal dumping of industrial wastes: the situation 15 years after the judicial intervention. Sci Total Environ 762:144100. https://doi.org/10.1016/j.scitotenv.2020.144100

Wang S, Yao Y, Wang J et al (2025) Advancing Stress-Resilient rice: Mechanisms, Genes, and breeding strategies. Agriculture 15. https://doi.org/10.3390/agriculture15070721

Wu D, Zhang Z, Wang Z (2024) Impact of manganese mining on potentially toxic elements pollution and bioaccumulation in spirogyra varians and hydrilla verticillata in the Xiaojiang river. Environ Geochem Health 46:381. https://doi.org/10.1007/s10653-024-02171-4

Xing W, Liu H, Banet T et al (2020) Cadmium, copper, lead and zinc accumulation in wild plant species near a lead smelter. Ecotoxicol Environ Saf 198:110683. https://doi.org/10.1016/j.ecoenv.2020.110683

Yan H, Wang B, Zheng K et al (2025) Integrated analysis of Heavy-Metal pollution in three Gorges reservoir sediments: Spatial Distribution, source Apportionment, and ecological risk assessment. Water 17. https://doi.org/10.3390/w17192852

Zhao Q, Liu H, Wu L et al (2024) Metal(loid) uptake and physiological response of Coix lacryma-jobi L. to soil potentially toxic elements in a polluted metal-mining area. Sci Rep 14:18833. https://doi.org/10.1038/s41598-024-69652-5

Zhou W, Wang H, Jiang H et al (2025) Manganese phytoremediation potential of Koelreuteria paniculata: detoxification Mechanisms, chemical Speciation, and ultrastructural adaptations. Plants 14. https://doi.org/10.3390/plants14182867

Authors and Affiliations

Shakeel Ahmed Talpur[1,2,3] · Simonetta Cristina Di Simone[4] · Aziz Ahmed[5] · Hafeez Ahmed Talpur[6] · Muhammad Yousuf Jat Baloch[7] · Francesco Stoppa[1,2] · Luigi Menghini[4] · Beatrice Maria Sole Giambastiani[3] · Gianluigi Rosatelli[1,2]

✉ Shakeel Ahmed Talpur
shakeel.talpur@unich.it

✉ Gianluigi Rosatelli
g.rosatelli@unich.it

1 DiSPUTer, Department of Psychological, Health and Territory Sciences, University "G. d'Annunzio", Chieti-Pescara, Chieti 66100, Italy

2 DATA – U.D'A Analytical High-Tech Laboratory, "G. d'Annunzio" University, Chieti 66100, Italy

3 Department of Biological, Geological, and Environmental Sciences, Ravenna Campus, University of Bologna, Bologna, Italy

4 Botanic Garden "Giardino Dei Semplici", Department of Pharmacy, "Gabriele d'Annunzio" University, Chieti, Italy

5 Centre for Environmental Sciences, University of Sindh, Jamshoro 76080, Sindh, Pakistan

6 Department of Engineering and Geology, University of "G. d' Annunzio", Chieti-Pescara, Chieti, Italy

7 School of Environmental Science and Engineering, Shandong University, Qingdao 266237, People's Republic of China